Seismic Response Comparison of Fixed-Base and Base-Isolated 8-Story Buildings with Frame and Shear Wall Systems

Ilham Nurhuda*, Windu Partono, Rico Fernando Onggowarsito, Revanza Aby Pradana,

Faishal Najwan Ahmad, Junia Anisa Marizki

Department of Civil Engineering, Diponegoro University, Semarang, Indonesia

Received 05 January 2026; revised 29 March 2026; accepted 01 April 2026

DOI: https://doi.org/10.46604/aiti.2026.16055

Abstract

This study investigates the effects of different lateral load-resisting systems on engineering demand parameters (EDPs) and evaluates the suitability of spectral acceleration (Sa) as an intensity measure for predicting their seismic response. Eight-story reinforced concrete buildings with four configurations—fixed-base moment-resisting frame, fixed-base dual system with shear walls, base-isolated moment-resisting frame, and base-isolated dual system with shear walls—were analyzed. The seismic responses are obtained through nonlinear time-history analyses using 11 ground motion records scaled to match the site conditions. Four key response parameters are examined: maximum lateral displacement, interstory drift, floor acceleration, and base shear. Overall, the base-isolated dual system exhibited the best performance across all response parameters. In addition, Sa can be reasonably used to estimate floor acceleration in frame structures. However, the use of Sa to estimate floor acceleration in dual systems with shear walls tends to underestimate the actual response.

Keywords: base isolation, frame, mid-rise buildings, shear wall, time history

1. Introduction

Earthquakes are among the natural disasters that frequently cause severe damage to buildings and result in significant loss of life. The estimation of earthquake-induced losses generally involves predicting the likelihood of earthquake occurrence, assessing the vulnerability of buildings to seismic events, estimating the potential damage, and quantifying the resulting losses. Within this framework, the estimation of earthquake intensity and the vulnerability of buildings to seismic hazards are key aspects in determining the extent of losses [1].

Liao et al. [2] investigated several earthquake intensity measures (IMs), including peak ground acceleration (PGA), peak ground velocity (PGV), specific energy density (SED), and spectral response parameters from single-degree-of-freedom (SDOF) analysis, such as Sa, to identify the most suitable IM for assessing the seismic resilience of buildings. The case study was carried out on eight-story reinforced concrete structures with an MRF system. The structural response was evaluated using two commonly used engineering demand parameters (EDPs), namely maximum interstory drift ratio (MIDR) and maximum floor acceleration. The correlation between IMs and EDPs was analyzed using double-logarithmic regression. The results indicated that PGV and Sa are the most effective seismic IMs for assessing seismic resilience.

This study uses Sa as the seismic IM to evaluate the EDPs of mid-rise structures. Mid-rise buildings, which typically consist of six to ten stories and are commonly found in urban areas, represent one of the building types most vulnerable to

* Corresponding author. E-mail address: ilham@live.undip.ac.id

earthquake damage [3]. These buildings generally exhibit fundamental vibration periods ranging from 0.5 to 1.5 s, a range that closely coincides with the predominant periods of strong ground motions generated by megathrust earthquakes. In addition, seismic motions within this period range are often associated with soft soil conditions, which can further amplify structural responses within similar frequency bands [4]. The study by Demirel et al. [4], conducted after the 2020 Samos earthquake, supports the observation by showing that, among 140 reinforced concrete buildings with 7-12 stories in the Bayraklı district, severe damage and collapse predominantly occurred in 8-9 story buildings. One of the contributing factors is that the soil in Bayraklı has a dominant period of approximately 1.0-1.6 s, with a time-averaged shear-wave velocity in the upper 30 m of the ground (Vs30) ranging from 180 to 400 m/s.

In this study, a site in Yogyakarta, Indonesia, was selected to represent soft soil conditions. The city is located in the southern part of Java Island and is exposed to seismic risks originating from three main sources: the offshore southern Java megathrust zone [5], the Opak Fault [6], and ground motions induced by volcanic activity [7]. The subsurface soil conditions in Yogyakarta generally consist of thick volcanic and alluvial deposits, characterized by low shear-wave velocity (Vs) and long predominant site periods (Ts) [8]. These conditions tend to amplify ground motions within frequency ranges close to the fundamental periods of mid-rise buildings, thereby increasing the potential for resonance effects. A notable earthquake event that caused severe damage to several mid-rise reinforced concrete buildings in Yogyakarta was the Mw 6.4 earthquake of 27 May 2006, which originated from the Opak Fault [6]. With the increasing demand for mid-rise buildings driven by ongoing urban development in Yogyakarta, there is a growing need to enhance the seismic safety and resilience of buildings against potential future earthquakes.

A common method to increase the seismic resistance of mid-rise buildings is the use of shear walls to increase the lateral stiffness of the structure. However, the presence of shear walls makes the structure more vulnerable to higher-mode vibrations, which can lead to the concentration of seismic forces within the wall elements and potentially result in brittle failure [9]. Another technique for improving the seismic performance of buildings is the implementation of base isolation systems in frame structures to decouple the superstructure from ground motion [10]. In base-isolated buildings, the superstructure is allowed to move almost uniformly across all floors. Although base isolation effectively reduces the seismic energy transmitted to the superstructure, the displacement of the isolators must be carefully limited to prevent overturning moments and structural instability [11]. Consequently, base-isolated structures may still experience considerable strain due to these deformation constraints.

The combined use of shear wall systems and base isolation offers significant potential for minimizing seismic effects on buildings. The base isolation system primarily functions to reduce the seismic energy transmitted to the superstructure, while shear walls are designed to enhance the lateral stiffness of the superstructure. Despite the promising protective capacity of combining shear walls with base isolation, their combined seismic behavior and effectiveness have not been extensively investigated, particularly within the framework of nonlinear performance-based analyses.

This study investigates the nonlinear seismic behavior of eight-story reinforced concrete buildings representing mid-rise structures. The buildings are modeled using two types of lateral load-resisting systems, namely the MRF system and the dual system with shear walls. Each structural system is analyzed under two configurations: fixed-base and base-isolated conditions. The inelastic behavior of the structure is modeled by defining plastic hinges at the ends of beams and columns to realistically represent structural nonlinearities. Subsequently, the structures are analyzed using ground acceleration records that represent the seismic conditions in Yogyakarta, which is selected as the study area. This study quantifies several key seismic response parameters, including maximum lateral displacement, interstory drift, floor acceleration, and base shear.

In addition, this study evaluates the use of Sa as a seismic IM for structural systems with different dynamic characteristics, namely moment-resisting frames (MRF) and dual systems with shear walls (SW). Unlike previous studies, which generally

focus on the relationship between intensity measures and engineering demand parameters (IM–EDP) within a single structural system, this study investigates differences in structural behavior across different systems and examines the relationship between Sa and maximum floor acceleration in these systems. Furthermore, this study considers not only the two commonly used EDPs: maximum interstory drift and maximum floor acceleration, but also extends the evaluation to four EDPs, namely maximum lateral displacement, interstory drift, floor acceleration, and base shear, thereby providing a more comprehensive assessment of seismic effects on different structural systems.

2. Methodology

This study follows the research workflow illustrated in Fig. 1. The investigation was conducted on four building models representing different lateral load-resisting systems and base conditions, namely: (1) MRF-F, a reinforced concrete moment-resisting frame structure with a fixed-base condition; (2) MRF-I, a reinforced concrete moment-resisting frame structure equipped with a base isolation system; (3) SW-F, a dual system consisting of reinforced concrete frames and shear walls with a fixed-base condition; and (4) SW-I, a dual system combining reinforced concrete frames and shear walls with base isolation. In the subsequent stage, ground acceleration records were selected and scaled to match the target response spectrum at the study site [12].

Each structural model was then analyzed using nonlinear time-history analysis (NTHA) under the selected ground motions. From these analyses, key seismic EDPs were recorded, including the fundamental period, maximum displacement, interstory drift, floor acceleration, and base shear. The results were subsequently compared and discussed to evaluate the influence of structural system type and the implementation of base isolation on overall seismic performance.

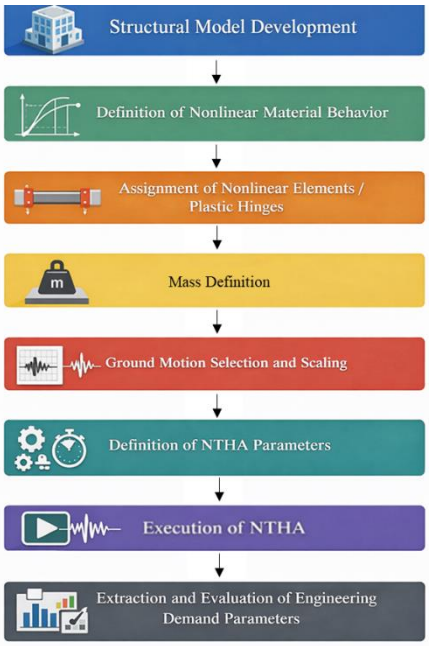

Fig. 1 Research workflow

2.1 Structural models

The buildings analyzed in this study are eight-story reinforced concrete (RC) structures designed in accordance with the Indonesian Standards SNI 2847 [13] and SNI 1726 [14]. The moment-resisting frame structures, MRF-F and MRF-I, share the same structural plan, as shown in Fig. 2. The building plan is rectangular, with a length of 56.4 m and a width of 22.0 m. The structural layout is uniform from the ground floor to the roof, with a total structural height of 33.6 m and an average story height of 4.2 m. Structural modeling and analysis were carried out using MIDAS Gen [15]. The beams and columns were

modeled as frame elements, while the shear walls were represented using shell elements. The reinforced concrete has a compressive strength of f'c = 35 MPa, and the reinforcing steel has a yield strength of fy = 420 MPa. The hysteretic behavior of plastic hinges was defined using moment-rotation relationships in accordance with FEMA 356 [16], as illustrated in Fig. 3. The dimensions and yield strength of each structural element in MRF-F and MRF-I are presented in Table 1.

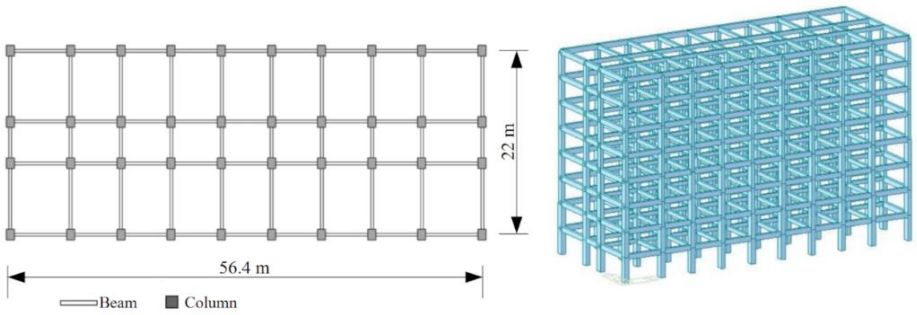

Fig. 2 Structural plan and isometric view of MRF-F and MRF-I buildings

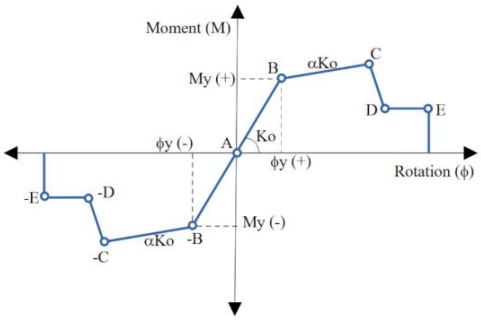

Fig. 3 Moment-rotation hysteresis behavior of plastic hinges

Table 1 Element properties of MRF-F and MRF-I structures

Element ID	Section Size (mm)	Element Type	Positive Yield Strength	Negative Yield Strength
B1A	600 × 900	Beam	My = 1399.5 kN·m	My = 1747.8 kN·m
B1B	600 × 900	Beam	My = 1398.5 kN·m	My = 1631.9 kN·m
B2A	400 × 700	Beam	My = 575.7 kN·m	My = 835.9 kN·m
B2B	400 × 700	Beam	My = 575.7 kN·m	My = 835.9 kN·m
B3A	600 × 900	Beam	My = 1398.5 kN·m	My = 1631.9 kN·m
B3B	600 × 900	Beam	My = 1749.1 kN·m	My = 1864.9 kN·m
B4A	500 × 700	Beam	My = 673.4 kN·m	My = 1025.6 kN·m
B4B	500 × 700	Beam	My = 858.2 kN·m	My = 1026.7 kN·m
K1	1200 × 800	Column	My = 3966.0 kN·m Mz = 2706.0 kN·m	My = 3966.0 kN·m Mz = 2706.0 kN·m
K2	1200 × 800	Column	My = 3136.0 kN·m Mz = 2073.0 kN·m	My = 3136.0 kN·m Mz = 2073.0 kN·m
K3	1200 × 800	Column	My = 2476.0 kN·m Mz = 1641.0 kN·m	My = 2476.0 kN·m Mz = 1641.0 kN·m

The dual-system structures, SW-F and SW-I, represent combined MRF and shear wall systems, with plan configurations shown in Fig. 4. The structural layout is uniform from the ground floor to the roof, with a length of 43.5 m and a width of 24.6 m. The total building height is 36.5 m, with an average story height of 4.5 m. The dimensions of the structural elements and their yield capacities in SW-F and SW-I are summarized in Table 2. The hysteretic behavior of plastic hinges is defined in accordance with FEMA 356 [16]. All modeling and analyses were carried out using MIDAS Gen [15].

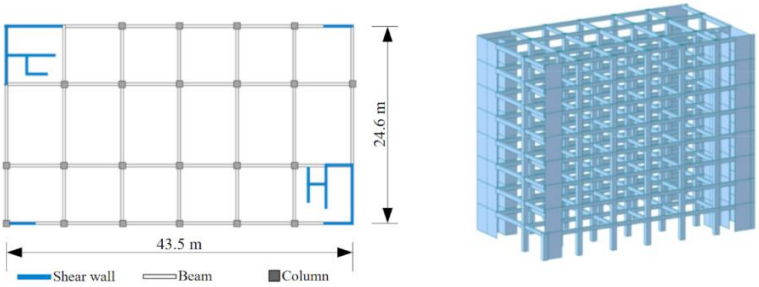

Fig. 4 Structural plan and isometric view of SW-F and SW-I buildings

Table 2 Element properties of SW-F and SW-I structures

Element ID	Section Size (mm)	Element Type	Positive Yield Strength	Negative Yield Strength
B1	400 x 800	Beam	My = 575.3 kN m	My = 1069.3 kN·m
B1A	500 x 800	Beam	My = 678.5 kN·m	My = 1571.7 kN·m
B2	400 x 700	Beam	My = 370.7 kN·m	My = 715.1 kN·m
B2A	400 x 700	Beam	My = 724.7 kN·m	My = 1125.1 kN·m
K1	900 x 900	Column	My = 1603.0 kN·m Mz = 1603.0 kN·m	My =1603.0 kN·m Mz = 1603.0 kN·m
SW1	400 x 7250	Shearwall	Fz = 8014.7 kN	Fz = 8014.7 kN
SW2	400 x 6500	Shearwall	Fz = 7178.0 kN	Fz = 7178.0 kN
SW3	400 x 3500	Shearwall	Fz = 3831.4 kN	Fz = 3831.4 kN

The base isolation system employed in this study consists of lead rubber bearings (LRBs) installed beneath all base columns and shear walls. The hysteretic behavior of the isolators was modeled using a bilinear hysteresis model [17], as shown in Fig. 5, and the mechanical properties of the isolators are summarized in Table 3. The isolator properties were designed to withstand ground motions corresponding to the maximum considered earthquake (MCER) level, while the superstructure was analyzed under ground motions representing the design basis earthquake (DBE) level.

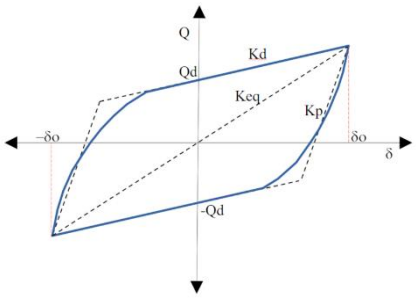

Fig. 5 Bilinear hysteresis model for LRB isolators

Table 3 Mechanical properties of LRB isolators

Isolator properties	MRF	SW
Maximum vertical load, Vmax (kN)	5530	8080
Characteristic shear strength, Qd (kN)	242	106
Post yield stiffness, Kd (kN/m)	1.26×10^3	1.78×10^3
Lead core stiffness, Kp (kN/m)	12.6×10^3	16.3×10^3

Before conducting the time-history analysis, several parameters were verified using static analysis, including the adequacy of member dimensions and reinforcement, beam deflection under gravity loads, and interstory drift ratios. In addition, the contribution of shear walls to the total base shear was evaluated. Live and dead loads were determined in accordance with SNI 1727 [18], while seismic loads were analyzed based on SNI 1726 [14] using the equivalent static method.

Structural strength analysis was performed in accordance with SNI 2847 [13], where all demand forces obtained from the structural analysis must be less than the design strength of the members, i.e., Mu < φMn, Vu < φVn, and Pu < φPn. Column capacities were also evaluated using axial force–bending moment interaction diagrams to ensure that the demand combinations remained within the safe region. The results of the static analysis indicate that all structural elements are capable of resisting the design loads in accordance with the Indonesian standards [13].

In addition, the vertical deflection of all beams is less than L/240, satisfying the requirements of SNI 2847 for total loads. The evaluation of interstory drift ratios from the static analysis shows that all structural types, namely MRF and SW systems, remain below 0.01, which is within the allowable drift limits specified in the code [14]. The base shear check indicates that the shear walls resist 69% and 61% of the total lateral forces in the two orthogonal directions of the structural plan.

2.2 Seismic hazard and site conditions

The buildings analyzed in this study are located in the Yogyakarta Basin, which is characterized by medium to soft soil conditions. Fig. 6 illustrates the building location on the map of average Vs30 within the top 30 m of the soil profile, as well as the map of resonant site frequency (F_0) in the Yogyakarta Basin. As shown in Fig. 6(a), most areas of Yogyakarta are represented by brown to red colors, indicating soft to medium soil conditions based on average Vs30 values of less than 250 m/s [19]. These soil conditions are consistent with the resonant site frequency (F_0) values presented in Fig. 6(b), where the Yogyakarta Basin exhibits F_0 values ranging from approximately 0.5 to 2 Hz in the reddish-colored regions of the map [8]. The resonant frequency F_0 corresponds to soil periods ranging from 0.5 to 2.0 s, which are generally associated with alluvial soft soils. Under these conditions, seismic vibrations tend to be amplified due to the oscillation of soft soil layers overlying bedrock. This soil period also corresponds to the fundamental periods of the mid-rise structures investigated in this study.

This study uses Sa as the seismic IM to scale ground motions at the study site in accordance with SNI 1726 [14]. The corresponding spectral response acceleration parameters for the short period (Sa_{SMS}) and the 1-second period (Sa_{SM1}) at the site are 1.175g and 0.904g, respectively. The MCER response spectrum and the DBE response spectrum for the region are shown in Fig. 7. The corner periods, T_0 and T_S, as indicated in the figure, are 0.154 s and 0.769 s, respectively.

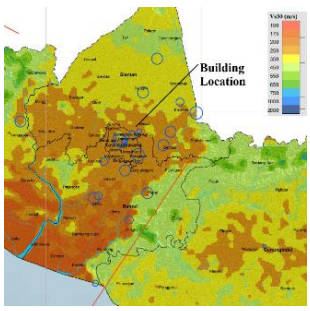

(a) Vs30 map of Yogyakarta [19]

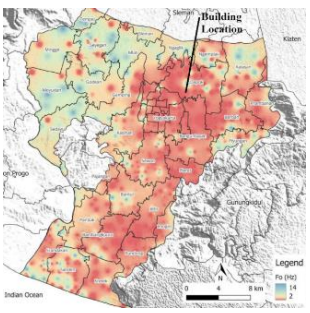

(b) Resonant site frequency (F_0) map of the Yogyakarta Basin [8]

Fig. 6 Building location shown on maps

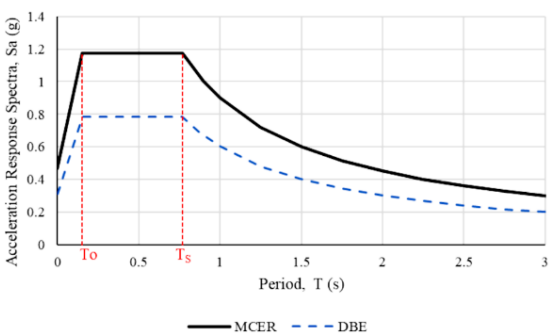

Fig. 7 MCER and DBE response spectra at the building site based on SNI 1726 [14]

2.3 Ground motion selection and scaling

The selected ground motions represent three earthquake source types: shallow crustal, Benioff (intraslab), and megathrust events. The corresponding magnitude-distance parameters at the building site were obtained from the deaggregation map [20], as summarized in Table 4. The average Vs30 at the site, calculated from the NSPT data, ranges between 230 and 250 m/s, which is consistent with the Vs30 distribution shown previously in Fig. 6. A total of 11 ground-motion records [21-22] were selected for this study, as listed in Table 5, and were subsequently scaled to match the target acceleration response spectrum at the building site.

Table 4 Summary of magnitude-distance parameters from seismic deaggregation [20]

Source Type	Magnitude (Mw)	Distance (km)
Shallow crustal	6.4	20
Benioff (intraslab)	7.2	80
Megathrust	8.0	100

Table 5 Selected ground-motion records used in the analysis

Source Type	Event	Location	Year	Magnitude (Mw)	Distance (km)	Vs30 (m/s)
Strike-slip	Imp. Valley 1	California	1979	6.53	22.03	242.05
Strike-slip	Chi-Chi	Taiwan	1999	6.20	21.67	258.89
Strike-slip	Imp. Valley 3	California	1979	6.53	21.98	249.92
Intraslab	Nicaragua	Central America	2014	7.32	113.65	281.00
Intraslab	South Sanriku	Japan	2003	7.03	113.57	234.80
Intraslab	Miyagi P1	Japan	2011	7.15	116.74	256.20
Intraslab	Miyagi P2	Japan	2011	7.15	85.48	234.80
Interface	Ibaraki-Off	Japan	2011	7.92	129.28	238.70
Interface	Tokachi-Oki 1	Japan	2003	8.29	132.53	242.25
Interface	Tokachi-Oki 2	Japan	2003	8.29	151.68	240.50
Interface	Tokachi-Oki 3	Japan	2003	8.29	125.07	240.45

2.4 Nonlinear time history analysis

The nonlinear time-history modeling and analysis were performed using MIDAS Gen [15]. The analysis procedure involved developing the structural model, defining the structural mass, specifying the nonlinear material behavior, and assigning plastic hinges to the structural elements, with models and properties as described in the previous subsection. Subsequently, ground motions were selected and scaled, and the time-history analysis parameters were defined prior to performing the time-history analysis.

The time-history analysis was carried out using direct integration based on the Newmark method. This method is widely used due to its good numerical stability. The Newmark parameters adopted were $\beta = 0.25$ and $\gamma = 0.5$. A time step of $\Delta t = 0.01$s was used, and the total analysis duration was set to 10 s to ensure computational efficiency. Damping was defined as proportional to mass and stiffness with a ratio of 5%, which is commonly used in the dynamic analysis of reinforced concrete structures. The analysis was performed automatically by MIDAS Gen until convergence was achieved at each time step.

The analysis was conducted for all structural models, and each structure was subjected to 11 scaled ground motion records. During the dynamic analysis, several EDPs were recorded, including floor displacements, maximum interstory drift ratios, maximum floor accelerations, and base shear in the x and y directions. The structural responses were recorded at each time interval Δt throughout the time-history analysis. The obtained response data were then evaluated for each type of EDP to investigate the characteristics of the dynamic response and to compare the responses of different structural systems.

3. Results

In general, the SW structures exhibit shorter fundamental periods and smaller maximum displacements than the MRF structures, while exhibiting higher floor accelerations and base shear. The use of base isolation increases the structural fundamental period and maximum displacement, particularly in SW structures, while reducing floor acceleration and base shear.

3.1 Natural periods of structures

The fundamental period of a structure represents its dynamic characteristics, which determine the deformation pattern and vibration response under dynamic loading [23]. The results of the fundamental period analysis for the four structural models examined in this study are presented in Table 6. It can be observed that the fundamental period of the SW Fixed structure falls within the region of maximum spectral acceleration, with all period values T < Ts (0.769 s). In contrast, the other structures, namely MRF-F, MRF-I, and SW-I, have fundamental periods greater than Ts. The influence of these differences in structural periods will be further discussed based on the engineering demand parameters obtained.

Table 6 Fundamental and higher mode periods of fixed-base and base-isolated structures

Building model	Period		
	Mode 1 (translation)	Mode 2 (translation)	Mode 3 (rotation)
MRF Fixed	0.959 s	0.882 s	0.797 s
MRF Isolated	2.563 s	2.503 s	2.418 s
SW Fixed	0.734 s	0.708 s	0.467 s
SW Isolated	2.543 s	2.499 s	2.047 s

3.2 Maximum lateral displacement

The analysis results show variations in maximum displacement values obtained from different ground-motion records. To represent the data variability independent of its statistical distribution, the results are expressed using the median, the 16th percentile (P_{16}), and the 84th percentile (P_{84}). Under a normal distribution, P_{16} and P_{84} correspond approximately to the mean minus one standard deviation and the mean plus one standard deviation, respectively [24].

Fig. 8 presents the variability of maximum roof displacement, which corresponds to the location exhibiting the largest displacement in both the MRF and dual system (SW) structures. The results indicate that the range of variation in base-isolated structures (MRF-I and SW-I) is wider than that in the fixed-base structures (MRF-F and SW-F). This occurs because the use of base isolation makes the structure more flexible and thus more sensitive to seismic excitation. Nevertheless, the larger maximum displacement observed in base-isolated structures has less detrimental impact on the overall structural response, since a significant portion of this displacement originates from the movement of the base isolators rather than from deformation of the superstructure itself [25]. Table 7 summarizes the base-floor and roof displacements for the four structural models.

3.3 Floor accelerations

Floor acceleration not only influences the seismic forces acting on each floor but also affects the performance of non-structural components, such as piping systems, suspended ceilings, equipment, furniture, and even the comfort and safety of occupants [26]. In this study, the maximum floor acceleration at each story was determined as the absolute peak horizontal acceleration obtained from all scaled ground-motion records consistent with the DBE response spectrum. The analytical results are presented in Fig. 9.

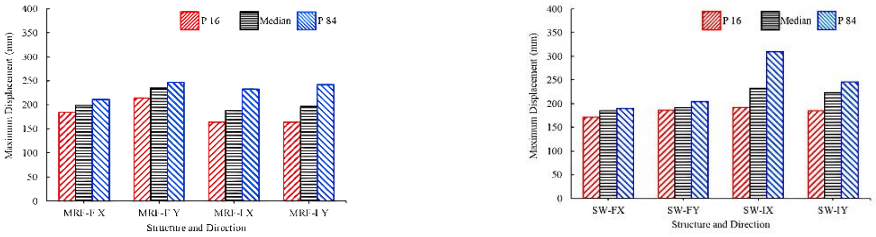

(a) MRF structures (b) SW structures

Fig. 8 Variation of maximum roof displacement (median, P_{16}, and P_{84})

Table 7 Lateral displacements of fixed-base and base-isolated structures

Location	MRF-FX (mm)	MRF-FY (mm)	MRF-IX (mm)	MRF-IY (mm)	SW-FX (mm)	SW-FY (mm)	SW-IX (mm)	SW-IY (mm)
Roof (δA)	199	234	188	197	185	191	233	223
Base (δB)	0	0	137	130	0	0	195	190
Difference (δA-δB)	199	234	51	67	185	191	38	33

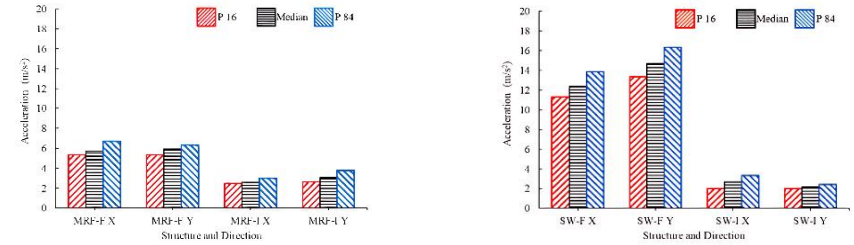

(a) Maximum floor acceleration of MRF structures (b) Maximum floor acceleration of SW structures

Fig. 9 Maximum floor acceleration

3.4 Base shear

The magnitude of base shear (V_b) is primarily influenced by the building mass (m) and the seismic acceleration (a) experienced by the structure. The building mass (m) is calculated based on the total building weight (W_t), which includes the dead load plus 25% of the live load, divided by the gravitational acceleration (g). To express the base shear in a non-dimensional form, the ratio of V_b to W_t is used. As shown below, the ratio V_b / W_t represents the acceleration demand (a_d) expressed in units of gravity (g). The resulting values of V_b / W_t for the 16th percentile (P_{16}), median, and 84th percentile (P_{84}) are presented in Fig. 10.

$$\frac{V_b}{W_t} = \frac{a_d}{g} \tag{1}$$

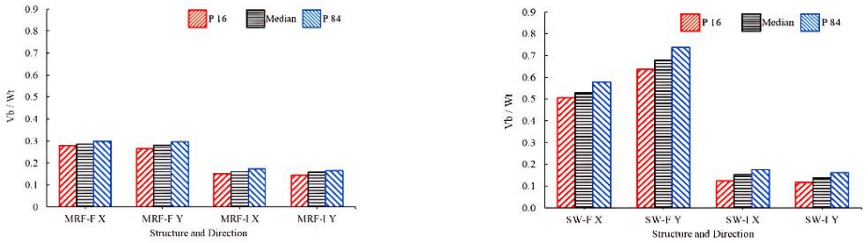

(a) MRF structures (b) Dual systems with shear walls (SW)

Fig. 10 Variation of base shear

4. Discussion

The influence of soil conditions and the assumptions adopted in this study are discussed in Section 4.1 to provide context for interpreting the obtained results. Subsequently, each EDP is examined, including the structural fundamental period, maximum lateral displacement, interstory drift, floor acceleration, and base shear. The discussion aims to identify the influence of structural characteristics on the investigated EDPs and their implications.

4.1 Effect of soil conditions

SNI 1726 classifies site conditions into four categories: soft soil, medium soil, hard soil, and rock [14]. Soft soil with low bearing capacity, when subjected to failure, can cause the overlying structure to experience permanent tilting. In contrast, stiff soil with high bearing capacity, when subjected to seismic excitation, may induce partial foundation uplift, allowing the structure to rock and dissipate seismic energy [27]. However, rocking predominantly occurs in shallow foundations, whereas in deeper foundations, foundation rotation is reduced, resulting in greater structural stability and smaller settlements.

The soil data used in this study indicate that the structures are located on medium soil. The influence of site conditions at the structural location is incorporated through the acceleration response spectrum in Fig. 7, which is used as a reference for scaling ground motion records, assuming that the structural foundation is perfectly fixed at the base. Although site conditions may also induce foundation rocking, the fixed-base assumption is adopted to focus the evaluation solely on the superstructure under consistent foundation conditions across all structural models.

This fixed-base approach does not account for potential foundation rocking or the increase in the fundamental period caused by soil flexibility. Therefore, the results of this study should be interpreted as the structural response to ground motions corresponding to the site conditions, without considering soil-structure interaction (SSI).

4.2 Effect of base isolation on the fundamental vibration period

In seismic analysis, the value of the fundamental period is a key parameter in determining the design seismic forces acting on the structure. The analysis results indicate that fixed-base structures (MRF-F and SW-F) have shorter fundamental periods compared to structures incorporating base isolation (MRF-I and SW-I). The first-mode period (T_1), which represents the fundamental vibration period, exhibits a greater increase in the dual-system model, with a ratio of T_1 (SW-I) / T_1 (SW-F) = 3.46, compared to the moment-resisting frame model, which has a ratio of T_1 (MRF-I) / T_1 (MRF-F) = 2.67. This difference occurs because the fixed-base dual system (SW-F) has higher stiffness than the MRF-F, whereas the periods of both structural types become nearly similar once base isolation is implemented. One of the primary objectives of employing base isolation is to lengthen the structural vibration period, thereby shifting it away from the dominant frequency range of earthquake ground motions associated with the site conditions. From this perspective, the use of base isolation in dual systems with shear walls is more effective in increasing the fundamental period than in moment-resisting frame systems.

4.3 Maximum lateral displacement

Maximum lateral displacement is commonly used to estimate the global drift ratio of a structure by assuming that the maximum displacement occurs at the roof level. This study investigates several eight-story mid-rise structures with different structural systems, namely fixed-base moment-resisting frame systems, fixed-base shear wall systems, and base-isolated structures, to examine whether the four analyzed structural systems exhibit maximum lateral displacement at the roof level. In addition, the study evaluates how the global drift ratio compares with the interstory drift ratio of the structures.

The maximum lateral displacement profiles, obtained as the median values from the eleven analyzed ground-motion records, are presented in Figs. 11-12. For the MRF structures, the use of base isolation significantly increases the lateral displacement up to approximately half of the building height, as shown in Fig. 11. This occurs because of the large lateral

movement at the base level resulting from the deformation of the base isolation system. However, if the base displacement is considered as the rigid-body movement of the isolation system and thus excluded from the structural deformation, the overall maximum lateral displacement of the base-isolated structure becomes smaller than that of the fixed-base structure. This indicates that the use of base isolation improves the seismic performance of the building by reducing the relative deformation demand on the superstructure.

A similar trend is also observed in the dual structural system (SW), as shown in Fig. 12. Base-isolated structures exhibit larger maximum lateral displacements than the corresponding fixed-base structures. However, when the response is evaluated in terms of relative maximum lateral displacement, defined as the difference between the lateral displacement at each floor and the base-floor displacement (see Table 7), the base-isolated structures demonstrate better performance.

The influence of base isolation on different structural systems is further illustrated in Table 7, which presents the differences between the maximum roof displacement (δA) and the maximum base-floor displacement (δB) for the MRF and dual-system (SW) structures. It can be seen that the dual system exhibits smaller displacement differences than the frame system, indicating that the presence of shear walls effectively reduces the lateral deformation of the structure.

The results of this study indicate that, although the distribution of maximum displacement across stories varies among the structures, the location of the maximum lateral displacement in all cases still occurs at the roof level. The maximum global drift ratio, calculated as the ratio of roof displacement to the total building height, is 0.7% for the MRF-F structure and 0.5% for the SW-F structure. These values are lower than the maximum interstory drift ratios reported in Section 4.4, indicating that the use of roof displacement to estimate drift results in an underestimation of structural deformation.

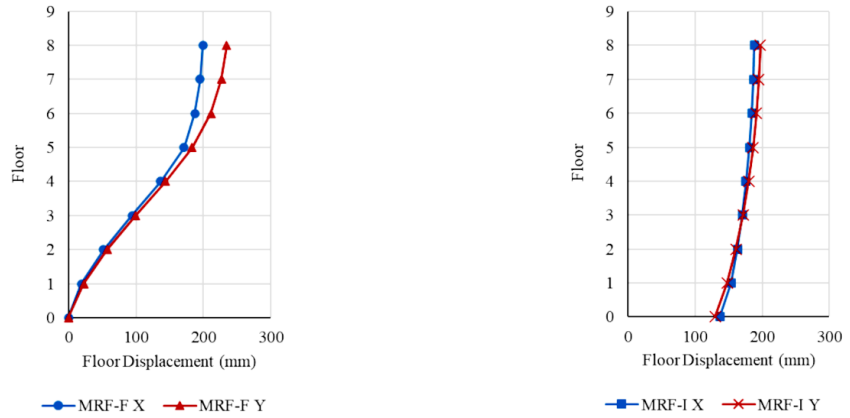

(a) Fixed moment-resisting frame (MRF-F) (b) Base-isolated moment-resisting frame (MRF-I)

Fig. 11 Maximum lateral displacement profiles of moment resisting frame structures (MRF)

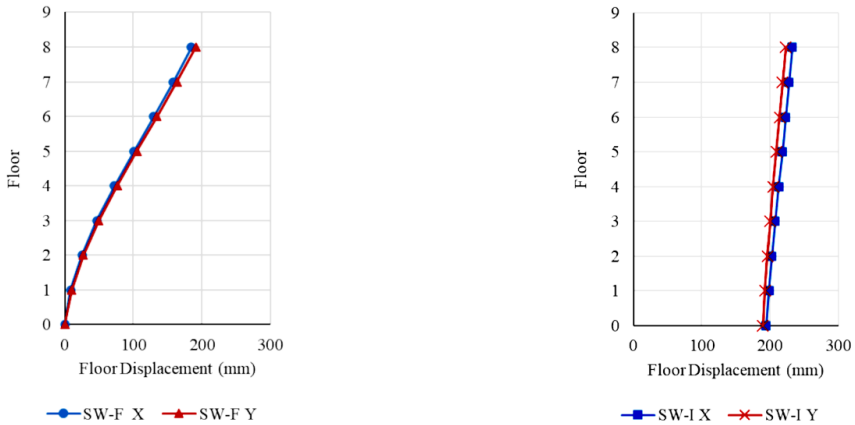

(a) Fixed dual system with shear wall (SW-F) (b) Base-isolated dual system with shear wall (SW-I)

Fig. 12 Maximum lateral displacement profiles of the dual system with shear wall (SW)

4.4 Interstory drift response and its implications for structural performance

Interstory drift is closely related to internal forces and the potential for structural damage at a certain story. The maximum interstory drift ratios at each story are illustrated in Figs. 13-14. In general, fixed-base structures exhibit larger interstory drift ratios than base-isolated structures for both the MRF system and the dual system with shear walls. The interstory drift ratios obtained from the analysis are approximately 1.0% for MRF-F and 0.7% for SW-F, which fall within the range typically associated with moderate damage [28]. The application of base isolation significantly reduces interstory drift along the height of the building compared with the fixed-base condition. The smaller drift ratios observed in the base-isolated structures indicate the effectiveness of the base isolation system in reducing the potential for both structural and non-structural damage. However, the interstory drift ratio profile of the MRF-I structure differs from that of the MRF-F structure, as the maximum interstory drift in the MRF-I occurs at the first story above the base isolation system. This behavior requires special attention in the design of base-isolated buildings to prevent potential failure at the first story.

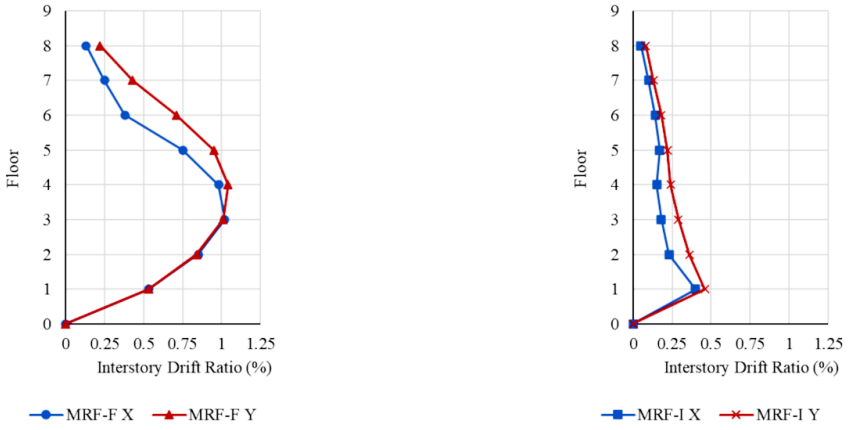

(a) Fixed-base MRF (MRF-F) (b) Base-isolated MRF (MRF-I)

Fig. 13 Maximum interstory drift ratio profiles of moment resisting frame (MRF)

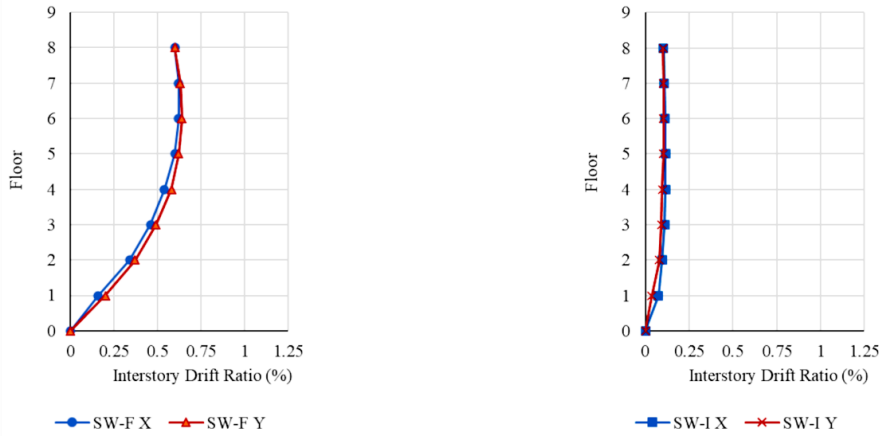

(a) Fixed-base dual system with shear wall (SW-F) (b) Base-isolated dual system with shear wall (SW-I)

Fig. 14 Maximum interstory drift ratio profiles of dual system (SW)

Notable differences are also observed in the interstory drift ratio profiles between the MRF-F and the SW-F. For the MRF-F structure, the maximum interstory drift ratio occurs around the mid-height of the building and then decreases significantly toward the roof. In contrast, for the SW-F structure, although the interstory drift ratio decreases after reaching its maximum value, the reduction is less pronounced, as shown in Figs. 13-14. The influence of shear walls can be clearly observed by comparing the magnitude of interstory drift ratios between the MRF and SW structures. The presence of shear walls significantly enhances the lateral stiffness of the structure, resulting in smaller interstory drift ratios in the dual system compared with those in the MRF system.

4.5 Floor acceleration response and the influence of higher-mode effects

Fig. 15 shows that the SW-F experiences maximum floor accelerations of up to approximately 2.5 times the roof acceleration of the MRF-F. This behavior occurs because the dual system with shear walls has greater lateral stiffness, causing its vibration to be influenced by higher frequencies and leading to higher-mode acceleration amplification. The effectiveness of base isolation in reducing floor acceleration is also clearly observed in Fig. 15, where base-isolated structures exhibit substantially lower maximum floor accelerations than their fixed-base counterparts. For the MRF-F structure, the median maximum roof acceleration obtained from the analysis was 5.9 m/s² (≈0.6g). This value decreased to 3.1 m/s² (≈0.31g), corresponding to a reduction of approximately 48%, after the implementation of base isolation.

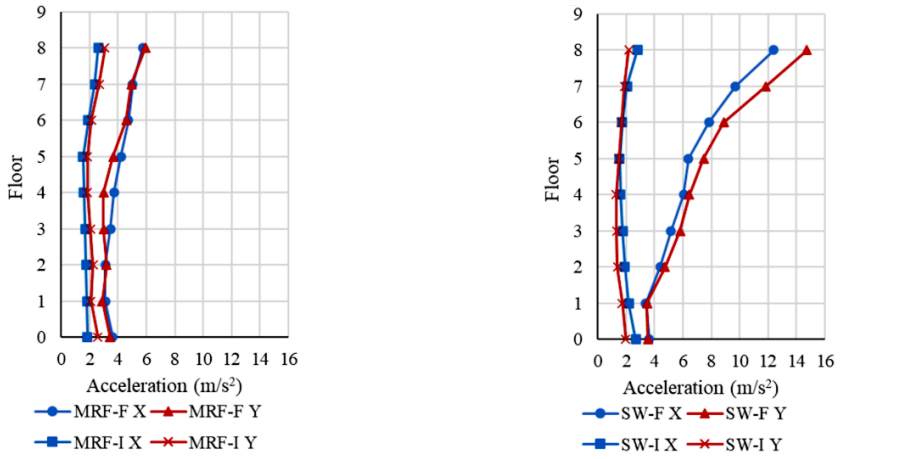

(a) MRF structures (b) Dual systems with shear walls (SW)

Fig. 15 Profile of maximum floor acceleration

The analysis employed time-history records scaled to match the DBE response spectrum. The corresponding DBE spectral acceleration for periods greater than TS (see Fig. 7) can be estimated using equation below. The fundamental period of the fixed-base MRF (0.959 s) yields a calculated spectral acceleration (SaDBE) of 0.63g, which closely matches the median maximum floor acceleration (0.6g) obtained from the nonlinear time-history analysis.

$$Sa_{DBE} = \frac{2}{3}\frac{S_{M1}}{T} \tag{2}$$

For the SW-F, the median maximum floor acceleration obtained from the analysis is 14.7 m/s² (≈1.5g). The fundamental period of the SW-F structure is 0.734 s, which falls within the constant-acceleration region of the DBE response spectrum (see Fig. 7), corresponding to a spectral acceleration (Sa_{DBE}) of 0.78g. This value is considerably lower than the maximum floor acceleration (1.5g) obtained from the nonlinear time-history analysis. Consequently, the use of the DBE response spectrum to estimate the maximum floor acceleration in such structures tends to underestimate the actual response. This discrepancy arises because the seismic response of dual systems with shear walls is strongly influenced by higher-mode effects, whereas the short-period spectral acceleration in the code-based spectrum is derived from an equivalent SDOF model that does not capture multi-mode behavior.

The base-isolated structures exhibit significantly longer fundamental periods, with T = 2.563 s for the MRF-I and T = 2.543 s for the SW-I. Using Eq. (2) and the DBE response spectrum, the corresponding spectral accelerations are Sa_{DBE} = 0.35g for the MRF-I and 0.36g for the SW-I. The nonlinear time-history analysis produced median maximum floor accelerations of 0.30g and 0.22g for the MRF-I and SW-I structures, respectively, which are in good agreement with those estimated from the DBE spectrum. This consistency can be explained by the fact that, in base-isolated systems, structural movement is concentrated at the isolation layer. This occurs because the lateral stiffness of the base isolation system is significantly lower

than that of the superstructure, thereby substantially reducing the acceleration demand parameters transmitted to the superstructure. It should be noted that this study considers an eight-story building as a representative mid-rise structure. The results may differ for high-rise buildings.

The analysis results indicate that the implementation of base isolation reduces the maximum floor acceleration by up to 48% in the MRF system and by approximately 85% in the dual system with SW. This reduction is greater than the acceleration reduction estimated based on the acceleration response spectrum, particularly for the frame–SW structures. Based on the spectral acceleration values, namely Sa_{DBE} MRF-F = 0.63g, Sa_{DBE} MRF-I = 0.35g, Sa_{DBE} SW-F = 0.78g, and Sa_{DBE} SW-I = 0.36g, the corresponding spectral-based acceleration reductions are 44% for the MRF structures and 54% for the SW structures.

The analysis indicates that, given the closer agreement between the floor accelerations obtained from time-history analysis and those predicted by spectral acceleration, spectral acceleration is more suitable for MRF structures. Accordingly, if the MRF-F structure is designed to have the same fundamental period as the SW-F structure, namely 0.734 s, the maximum floor acceleration estimated from spectral acceleration is 0.78g, resulting in a 55% reduction due to base isolation. However, this reduction remains smaller than that observed in the frame–SW structure based on time-history analysis with the same fundamental period, where the maximum floor acceleration reduction reaches 85%.

From a seismic protection perspective, the reduction in floor acceleration decreases the seismic vibrations transmitted to the structure and minimizes the potential for both structural and non-structural damage [25]. Furthermore, the decrease in floor acceleration leads to a reduction in inertial forces acting on the floors, thereby enhancing the overall seismic performance and safety of the building.

4.6 Influence of structural system on seismic base shear

The base shear (V_b) represents the total horizontal seismic force acting on a structure and plays an important role in the design of both the superstructure and the foundation. This study compares the base shear responses, expressed as the ratio of base shear to total building weight (V_b / W_t), of eight-story reinforced concrete buildings with different structural systems and base conditions, analyzed using the same set of ground-motion records. For the MRF-F structure, the base shear ratio (V_b / W_t) ranges from 0.28 to 0.30. These values are lower than the DBE spectral acceleration (Sa_{DBE}) calculated using the structure's fundamental period. This suggests that the base shear estimated using the equivalent static method for the MRF yields conservative results. Furthermore, the analysis shows that the implementation of base isolation significantly reduces the base shear in the MRF, with the V_b / W_t ratio decreasing to approximately 0.14-0.17, corresponding to a reduction of about 50% (Fig. 10).

For the SW-F, the 84th percentile value of the V_b / W_t ratio is 0.74, which is close to the DBE spectral acceleration (Sa_{DBE} = 0.78g) computed based on its fundamental period. A comparison of base shear between the SW-F and the MRF-F indicates that the base shear ratio of the SW-F structure is approximately 2.0 times higher than that of the MRF-F structure, as shown in Fig. 10.

The effect of base isolation on the dual system with shear walls is also clearly observed in Fig. 10, where the base shear is significantly reduced to approximately 0.12-0.17 W_t, corresponding to a reduction of about 80%. The larger reduction in base shear observed in the dual system compared with the moment-resisting frame indicates that the dual system with base isolation is more effective in reducing seismic base shear demand. Overall, these results demonstrate that the choice of structural system has a significant influence on the seismic forces transmitted to the superstructure and the foundation, and therefore plays a key role in determining the seismic performance of the structure.

5. Conclusions

This study investigated the nonlinear seismic response of eight-story reinforced concrete buildings with different structural systems and base conditions through nonlinear time-history analysis. The comparison between moment-resisting frame and dual systems with shear walls, under both fixed-base and base-isolated configurations, provides insights into the influence of structural characteristics on seismic response and the applicability of spectral acceleration in predicting floor acceleration. This study draws the following conclusions:

(1) The fixed-base dual system with shear walls more effectively reduces lateral displacement and interstory drift than the MRF structure. However, the inclusion of shear walls leads to higher floor acceleration and base shear demand.

(2) The lateral drift ratio calculated based on roof displacement and total building height is lower than the corresponding interstory drift ratios, therefore being unsuitable for estimating structural damage without modification.

(3) Base isolation effectively reduces interstory drift, maximum floor acceleration, and base shear in both structural systems. However, the maximum interstory drift in base-isolated MRF structures is concentrated at the first story above the isolation and requires careful detailing.

(4) The use of base isolation in dual systems with shear walls results in the best overall seismic performance, exhibiting the lowest values in all key response parameters, including relative lateral displacement, interstory drift, floor acceleration, and base shear. This configuration represents a promising solution for enhancing the seismic resilience of mid-rise buildings.

(5) Spectral acceleration (S_a) underestimates the maximum floor acceleration in dual systems with shear walls. Floor accelerations obtained from nonlinear time-history analysis can reach up to twice the S_a value. More accurate predictions can be achieved by incorporating higher-mode contributions into the spectral acceleration analysis.

This study employed an LRB base isolation system and considered only a single study site with specific soil conditions. Future research is recommended to investigate various base isolation technologies and different soil conditions to assess their effects on structural performance. In addition, this study focused solely on regular eight-story mid-rise buildings; further studies may extend the scope to include irregular building configurations.

Conflicts of Interest

The authors declare no conflict of interest.

References

[1] A. Du, X. Wang, Y. Xie, and Y. Dong, “Regional Seismic Risk and Resilience Assessment: Methodological Development, Applicability, and Future Research Needs – An Earthquake Engineering Perspective,” Reliability Engineering & System Safety, vol. 233, article no. 109104, 2023.

[2] J. Liao, D. Forcellini, J. Fang, and L. Sun, “An Entropy-Based Multi-Criteria Approach for Intensity Measure Selection in Seismic Resilience of Structures,” Resilient Cities and Structures, vol. 5, no. 1, pp. 1-13, 2026.

[3] O. C. Celik, M. B. C. Ulker, C. Gocer, S. Guntepe, O. Koz, M. M. Eyupgiller, et al., “Multidisciplinary Reconnaissance Investigation Covering Structural, Geotechnical, and Architectural Based Damage to Mid-rise Residential Buildings Following the February 6th, 2023 Kahramanmaraş, Türkiye Earthquake Doublets (M_w 7.8, M_w 7.6),” Soil Dynamics and Earthquake Engineering, vol. 182, article no. 108738, 2024.

[4] I. O. Demirel, A. Yakut, and B. Binici, “Seismic Performance of Mid-Rise Reinforced Concrete Buildings in Izmir Bayrakli after the 2020 Samos Earthquake,” Engineering Failure Analysis, vol. 137, article no. 106277, 2022.

[5] M. Megawati, K. F. Ma, P. F. Chen, D. Sianipar, and M. C. Hsieh, “Source Characterization of Intermediate-Depth Earthquakes in Southern Java, Indonesia,” Journal of Asian Earth Sciences, vol. 264, article no. 106040, 2024.

[6] V. Librian, M. Ramdhan, A. D. Nugraha, M. M. Mukti, S. Syuhada, B.-G. Lühr, et al., "Detailed Seismic Structure Beneath the Earthquake Zone of Yogyakarta 2006 (Mw ~6.4), Indonesia, from Local Earthquake Tomography," Physics of the Earth and Planetary Interiors, vol. 351, article no. 107170, 2024.

[7] B. Voight, E. K. Constantine, S. Siswowidjoyo, and R. Torley, "Historical Eruptions of Merapi Volcano, Central Java, Indonesia, 1768-1998," Journal of Volcanology and Geothermal Research, vol. 100, no. 1-4, pp. 69-138, 2000.

[8] B. Sunardi, Sismanto, E. Hartantyo, and M. Nukman, "Seismic Vulnerability in Yogyakarta Basin Based on HVSR Frequency Domain Window Rejection Algorithm," International Journal of Design & Nature and Ecodynamics, vol. 20, no. 4, pp. 813-823, 2025.

[9] M. Marius, "Seismic Behaviour of Reinforced Concrete Shear Walls with Regular and Staggered Openings after the Strong Earthquakes between 2009 and 2011," Engineering Failure Analysis, vol. 34, pp. 537-565, 2013.

[10] F. Naeim and J. M. Kelly, Design of Seismic Isolated Structures: From Theory to Practice, 1st ed., New York, USA: Wiley, 1999.

[11] J. Zhang, Y. Li, H. Yang, X. Ji, L. Gu, W. Li, et al., "Enhancing the Overturning Resistance Capacity of High Aspect Ratio Structure through Hybrid Base Isolation and Inter-storey Isolation," Soil Dynamics and Earthquake Engineering, vol. 187, article no. 108993, 2024.

[12] A. Demir, A. H. Kayhan, and M. Palanci, "Response-and Probability-Based Evaluation of Spectrally Matched Ground Motion Selection Strategies for Bi-directional Dynamic Analysis of Low-to Mid-rise RC Buildings," Structures, vol. 58, article no. 105533, 2023.

[13] Building Code Requirements for Structural Concrete and Commentary, SNI Standard 2847, 2019 (in Indonesian).

[14] Seismic Design Code for Building and Nonbuilding Structures, SNI Standard 1726, 2019 (in Indonesian).

[15] MIDAS IT, "Midas Gen: General Structural Analysis System for Buildings and General Structures," https://www.midasuser.com/en/product/gen, accessed in 2025.

[16] Prestandard and Commentary for the Seismic Rehabilitation of Buildings, FEMA Standard 356, 2000.

[17] Y. Domadzra, M. Bhandari, and M. Hasan, "Influence of Characteristics of Lead Rubber Bearing Isolator on the Seismic Response of a Base-Isolated Building," Journal of Structural Design and Construction Practice, vol. 30, no. 3, article no. 04025044, 2025.

[18] Minimum Design Loads and Associated Criteria for Buildings and Other Structures, SNI Standard 1727, 2020 (in Indonesian).

[19] A. Cipta, A. Solikhin, I. C. Priambodo, R. Robiana, H. Afif, et al., Local Site Atlas (Vs30) of Indonesia Based on Engineering Geomorphological Classification, 1st ed., Jakarta, Indonesia: Center for Volcanology and Geological Hazard Mitigation, Geological Agency, Ministry of Energy and Mineral Resources, 2022.

[20] PuSGeN, Indonesian Earthquake Hazard Deaggregation Map for the Design and Evaluation of Earthquake-Resistant Infrastructure, 1st ed., Jakarta, Indonesia: Directorate of Housing and Settlement Engineering, Directorate General of Human Settlements, Ministry of Public Works and Housing, 2022.

[21] T. D. Ancheta, R. B. Darragh, J. P. Stewart, E. Seyhan, W. J. Silva, B. S.-J. Chiou, et al., "NGA-West2 Database," Earthquake Spectra, vol. 30, no. 3, pp. 989-1005, 2014.

[22] Y. Bozorgnia, N. A. Abrahamson, S. K. Ahdi, T. D. Ancheta, L. A. Atik, R. J. Archuleta, et al., "NGA-Subduction Research Program," Earthquake Spectra, vol. 38, no. 2, pp. 783-798, 2022.

[23] I. Nurhuda, P. Sabdono, M. R. Afrizal, L. A. P. Pratama, and S. A. Faishal, "Empirical Formula for the Fundamental Period of Reinforced Concrete Moment Resisting Frames in Indonesia," Jurnal Teknik Sipil, vol. 32, no. 1, pp. 1-8, 2025.

[24] B. A. Bradley, "Design Seismic Demands from Seismic Response Analyses: A Probability-Based Approach," Earthquake Spectra, vol. 27, no. 1, pp. 213-224, 2011.

[25] O. H. Mohamed, B. Abderrachid, and O. Abdelhafid, "LRB System Performance Validation and Its New Design Approach for Conventional Buildings in Algeria," Practice Periodical on Structural Design and Construction, vol. 29, no. 3, article no. 04024029, 2024.

[26] N.G. Wariyatno, H. A. Lie, F.-P. Hsiao, and B. S. Gan, "Design Philosophy for Buildings' Comfort-Level Performance," Advances in Technology Innovation, vol. 6, no. 3, pp. 157-168, 2021.

[27] S. O. Khamesi and S. M. Mir Mohammad Hosseini, "A Numerical Study of Influential Parameters on Rocking Response of Shallow Foundations of Single Degree of Freedom (SDOF) Structures," Journal of Engineering Research, vol. 11, no. 2, article no. 100055, 2023.

[28] W.-I. Liao, C.-H. Loh, and K.-C. Tsai, "Study on the Fragility of Building Structures in Taiwan," Natural Hazards, vol. 37, no. 1-2, pp. 55-69, 2006.